Engineering Structures 298 (2024) 116934

Contents lists available at ScienceDirect

Engineering Structures

journal homepage: www.elsevier.com/locate/engstruct

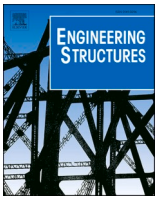

Vibration signature effects on damping identification of a RC bridge under ambient vibrations

Giacomo Zini *, Andrea Giachetti, Michele Betti, Gianni Bartoli

Department of Civil and Environmental Engineering, University of Florence, via di S. Marta 3 – I, 50139 Florence, Italy

ARTICLE INFO

Keywords:
Damping estimation
Short-span RC bridges
Spectral analysis
Traffic induced vibrations
Half-joints
Signal length

ABSTRACT

Experimental tests for dynamic identification of reinforced concrete (RC) bridges by means of Operational Modal Analysis (OMA) are increasingly used in common engineering practice. Nevertheless, especially when measurements are carried out under in-service conditions (i.e. under traffic induced vibrations), some drawbacks should be carefully considered, especially in the damping-ratio quantification. As a matter of fact, the estimation is affected by several factors: i) the length of the signals, ii) the non-stationarity of the input process, and iii) the dependence on the vibration amplitude. Even if the damping ratio is a key parameter in the bridge dynamics, a major part of these aspects has not been yet fully investigated to estimate reliable values.

Starting from a dynamic test program on a short-span RC bridge with half-joints in Italy, this paper investigates the issues mentioned above for the damping ratio estimation of the first two modes focusing on: i) the influence of the signal length, ii) the effects of the signals properties, and iii) their correlation with the vibration amplitude. Both the Stochastic Subspace Identification technique fed with the signal covariance (SSI-cov) and the Random Decrement technique (RD) have been used to compute the damping ratios from the collected signals. This paper shows how a convergence of the results cannot be attained by simply increasing the sample size, suggesting that the nature of the vibration itself influences the damping values. A negative, although weak, correlation between the damping ratio and the power of the signals indicates that several factors play a crucial role in the damping estimation in the short span RC bridges with half-joints.

1. Introduction

Most of the bridges across the European countries were built (or rebuilt) in a limited time after World War II, ranging from the 50 s to 70 s. During the same period, in the USA the "Greatest Decade" begun, providing the construction of thousands of km of highways, requiring several new bridges [1]. That golden era in bridge engineering, has now left worldwide thousands of bridges close or at the end of their design-life. In this scenario, dynamic tests [2,3] can be considered an important tool to increase the level of structural knowledge of the existing bridges. Among all the dynamic features that can be extracted from the vibration signatures, the damping ratio is a key parameter to describe the dynamic response, and can also be an attractive damage-sensitive feature to be considered in a Structural Health Monitoring (SHM) framework [4,5].

Nevertheless, even if the dynamic testing has become a mature research field the behaviour and the estimation of the damping ratio from Ambient Vibration Tests (AVTs) has not been extensively discussed yet. Such parameter can be considered as a measure of the energy dissipation during the AVTs arising from different physical phenomena and several factors can play an important role on its estimation. For instance, Zarafshan [6] classified those contributions as: i) material damping at a micro-scale level, ii) external damping at a macro-scale level (including the Coulomb friction and the damping in the joints), and iii) environmental damping (due to the interaction between the structure and soil, wind, water, etc.). To date, the main area of interest is the environmental damping, with many studies focused on the aerodynamic damping contribution in the case of long-span suspended bridges [7–10]. But, only Nagayama [11] found a positive correlation between the estimated damping and the root mean square of the recorded signals during the AVTs of the Hakuchō bridge in Japan. Considering other contributions, only few examples are available in literature for other bridge typologies. For instance, Lee [12] investigated the contribution to dissipation-induced damping at the boundaries in short-span bridges during strong motions to define a suitable equivalent viscous damping in seismic analysis. To test this method, a Finite

* Corresponding author.
E-mail addresses: giacomo.zini@unifi.it (G. Zini), andrea.giachetti@unifi.it (A. Giachetti), michele.betti@unifi.it (M. Betti), gianni.bartoli@unifi.it (G. Bartoli).

https://doi.org/10.1016/j.engstruct.2023.116934
Received 3 May 2023; Received in revised form 9 August 2023; Accepted 20 September 2023
Available online 31 October 2023

Element model was tuned to reproduce the time histories recorded during earthquakes with no structural damage. In addition, Schubert [13] investigated a light-weighted timber bridge, finding an increase in the damping due to the interaction between the deck and the asphalt. The research was conducted with dynamic tests on a scale model tested with different excitations.

To date, considering short-span reinforced concrete (RC) bridges, several researchers presented case studies of the AVTs under traffic vibrations [14–17] obtaining very scattered results ranging between 0.5 and 8 %, though not providing much information about the damping ratio estimation. This approach is commonly justified by the assumption that the damping ratio estimation is a complex task affected by several uncertainties (i.e. non-linearities, bias introduced by the identification techniques, etc.), thus the values are just reported without any additional discussion. Besides these cases, Li [18] reported the damping values identified in a huge dataset of 114 bridges in China, concluding that such results are scattered exhibiting a high-variability depending on the bridge typology.

Meantime, several techniques have been proposed in the last decades to improve the accuracy of the damping ratio estimation through ambient vibration tests. For instance, Gutenbrunner [19] performed sensitivity analysis using different techniques for the damping estimation, concluding that the Random Decrement (RD) [20] and the Stochastic Subspace Identification (SSI) [21] are the most reliable techniques. Nonetheless, those techniques assume a Gaussian white noise input loading the structural system. This assumption can be considered satisfied in the field of in-service measurements if the traffic properties (mass and speed of the vehicles, suspension systems, etc.) can be considered as random events [22]. Therefore, both the traffic characteristics and the recording time length can play a crucial role in the stationarity of the input random process, that may lead to considerable errors in the damping estimation of a bridge under service loads. Even if such issue can compromise the dynamic identification, only Brincker and Ventura (Brincker and Ventura 2015) proposed a rule of thumb to define the optimal signal length for AVTs.

From the literature review on this topic several gaps emerge: i) the damping identification of short span RC bridges has not been fully investigated, ii) the definition of a minimum time-length for the AVTs of bridges has not been provided yet, and iii) the sources of variability in the estimated damping ratios during AVTs has not been properly investigated yet. Aiming to investigate about these scientific gaps, this paper analysed and discussed the following topics: i) the bias on the damping estimation with respect to different signal lengths, ii) a recognition about minimum signal length to identify unbiased damping values, and iii) the correlation between the damping and the vibration signatures to verify if a clear dependence on the vibration amplitude can be observed for such bridge typology. To investigate the entries above listed, considering the complexity of the problem, only the first two modes identified from an extensive dynamic test program under ambient vibration on a short span RC bridge were considered. This assumption is justified by the fact that the first two modes are well-separated and excited during the AVTs, exhibiting high signal-to-noise ratio, thus the results can be considered as scarcely affected by external noises.

In the remainder of this paper, Section 2 provides a brief theoretical overview of the most frequently used techniques for damping estimation. Section 3 reports a description of the investigated RC bridge, together with the testing program and the adopted dynamic identification procedure. The results of the damping estimation are discussed in Section 4, while Section 5 analyses the influence of the window length and the correlation of the estimated damping to the vibration signatures. Section 6 concludes the paper, summarizing the outcome of this study.

2. Damping estimation: Brief theoretical background

The equations of motion representing the dynamic equilibrium at each time step t of a multi-degree of freedom system are:

$$\mathbf{M}\ddot{x}(t) + \mathbf{C}\dot{x}(t) + \mathbf{K}x(t) = F(t) \tag{1}$$

where $\mathbf{M}$, $\mathbf{C}$, $\mathbf{K}$ are the mass, damping and stiffness matrix respectively; $\ddot{x}(t)$, $\dot{x}(t)$, $x(t)$ are the accelerations, velocities, and displacements at each degree of freedom; $F(t)$ is the dynamic force acting on the system or the external input. When the additional damping sources are considered, the damping matrix does not satisfy the Caughey-O'Kelly's condition [23] and the structural system becomes non-proportionally damped, exhibiting complex eigenvalues and eigenvectors. Thus, the state-space format of the dynamic problem in Eq. (1) is expressed in the state-space formulation described in Eq. (2):

$$\begin{cases} \mathbf{A}\dot{u}(t) + \mathbf{B}u(t) = f(t) \\ x(t) = \mathbf{P}u(t) \end{cases}, \text{ with } u(t) = \begin{Bmatrix} \dot{x}(t) \\ x(t) \end{Bmatrix} \tag{2}$$

where the block matrices in the 2 N × 2 N state space are equal to:

$$\begin{aligned} \mathbf{A} &= \begin{bmatrix} \varnothing & \mathbf{M} \\ \mathbf{M} & \mathbf{C} \end{bmatrix}, \\ \mathbf{B} &= \begin{bmatrix} -\mathbf{M} & \varnothing \\ \varnothing & \mathbf{K} \end{bmatrix}, \\ f(t) &= \begin{Bmatrix} \emptyset \\ \mathrm{F(t)} \end{Bmatrix}, \\ \mathbf{P} &= [\emptyset \quad \mathbf{I}]. \end{aligned} \tag{3}$$

The modal properties of the system can be found by the eigenvalue decomposition of the inner product $-\mathbf{A}\hat{(}-\mathbf{1})\ \mathbf{B} \in \mathbb{C}^{2N\times 2N}$, obtaining the eigenvector $\boldsymbol{\varphi}_\mathbf{n} \in \mathbb{C}^{2N\times 2N}$ and the eigenvalue $\boldsymbol{\lambda}_\mathbf{n} \in \mathbb{C}^{2N\times 2N}$ matrices reported in Eq. (4).

$$\begin{aligned} \boldsymbol{\varphi}_\mathbf{n} &= \begin{bmatrix} \boldsymbol{\lambda}_\mathbf{n}\boldsymbol{\phi}_\mathbf{n} \\ \boldsymbol{\phi}_\mathbf{n} \end{bmatrix}, \\ \boldsymbol{\lambda}_\mathbf{n} &= \begin{bmatrix} \lambda_1 & \cdots & 0 \\ \vdots & \ddots & \vdots \\ 0 & \cdots & \lambda_{2N} \end{bmatrix}. \end{aligned} \tag{4}$$

In the underdamped systems the eigenvalues are complex conjugate, leading to the following expressions for the n-th mode damped circular frequency ω_{0n} and damping ratio ξ_n:

$$\begin{aligned} \omega_{0n} &= |\lambda_n| = \sqrt{\lambda_n \lambda_n^*}, \\ \xi_n &= -\frac{\Re e\{\lambda_n\}}{|\lambda_n|}. \end{aligned} \tag{5}$$

In Eq. (5) $\bullet^*$ stands for the complex conjugate operator.

When dealing with discrete time signals, collected with a sampling rate f_s, the Eq. (5) can be written as follows:

$$\begin{aligned} \omega_{0n} &= \frac{|\ln(\lambda_n)|}{\Delta \mathrm{t}}, \\ \xi_n &= -\frac{\Re e\{\ln(\lambda_n)\}}{\omega_{0n}\Delta \mathrm{t}}. \end{aligned} \tag{6}$$

where the discrete time step Δt at which the signals are sampled is equal to $\Delta t = 1/f_s$.

Commonly the parametric techniques operating in the time domain (SSI, AR, ARMA, ERA, ITD etc.) are based on fitting the state space model reported in Eq. (2) to a discrete statistical model, and the system matrices are used to estimate the poles λ_n and consequently the

continuous modal properties with the Eq. (6). Other methods (EFDD, RD, etc.) deal with the estimation of the correlation functions at each mode, and the damping ratios can be estimated as the decrement after each cycle. Thus the damping ratio can be estimated by the vibration signatures. Those readers interested in further details may consider [24,25] for more complete descriptions.

Within this paper the methods used for the damping identification are the Random Decrement (RD) and the Stochastic Subspace Identification (SSI). In the first case the damping is estimated by means of the RD functions, in the second the poles of the dynamic system in the state-space format can be calculated by fitting the discrete stochastic model to the collected data.

The RD method proposed by Cole was already tested on civil structures [26,27]. In this paper, the technique was applied on signals filtered around the first and the second mode after a Modal Assurance Criterion (MAC) [28] analysis, to obtain an estimation of each SDOF bell function. In particular, starting from the FDD results, the frequency band around the dominating peaks corresponding to the first two modes characterized by a MAC higher than 0.8 (e.g. [29]) were considered (it is to be observed that the MAC analysis was performed also considering the second singular value).

The SSI-cov [21], operating with the signal covariances in the time domain, requires the setting of some tuning parameters. This issue was tackled by means of a sensitivity analysis [30] that allows to minimize the bias on the results.

3. Investigated bridge and damping estimation (experimental program)

3.1. Bridge description

The experimental data considered in this study were obtained performing AVTs under traffic-induced vibrations on a straight-line six-span RC bridge with half-joints (or Gerber's joint) in the span C2. The bridge, called "Ponte Nuovo" (new bridge) (Fig. 1-a), crosses the Arno River near Florence (in the centre of Italy). It was almost completely rebuilt after World War II. Even if there is lack of information about the construction phase, additional maintenance works, which were made in the last decades, are still visible (Fig. 1-b). The bridge is characterized by one lane on a way (towards Signa) and two lanes on the opposite one (towards Lastra a Signa). As shown in Fig. 2-a, starting from Lastra a Signa, the first three spans are half-joints beams with a length of about 22.3, 30.9 and 22.3 m, respectively. The remaining spans towards Signa are simply supported beams of about 15.5 m.

The bridge deck is supported by five rectangular RC girders with variable rectangular cross-section and four RC cross-beams (two at the bearings and the other two at one and two third of the entire length, respectively). While at midspan of C2 the girder cross-section are about 0.37 × 1.27 m (Fig. 2-b), in the piles P1 and P2 the girder cross sections reach 1.47 m (Fig. 2-c). The transversal RC slab exhibits a cross section of about 0.20 m with more than 0.15 m of sand and gravel supporting the asphalt layers. Moreover, the cross-sections at the piles P1 and P2 are closed by another RC slab of about 0.1 m in the lower part of the girders which acts as a diaphragm. In the other three spans (C4-C5-C6) the girder cross-section is almost constant with dimensions equal to 0.37 × 1.27 m. Additional details about the RC bridge geometry can be found in [31].

Given that the current study focuses on the first three spans (C1-C2-C3) of the bridge, some additional information will be provided next. The piles over which the first three spans are laid are in the riverbed: the picture reported in Fig. 1-a was made during measurements, in the dry season, but depending on the precipitation all the piles can be underneath water level. On the Lastra a Signa side, few meters before the beginning of the bridge, a traffic light is installed; thus, two lines of cars often cover entirely the first three spans on the upstream side. Finally, it is worth noting that the road pavement is not regular and presents several unevenness at the beam expansion-joints, becoming more consistent near to the half-joints in the span C2.

(a) (b)

Fig. 1. Views of the Ponte Nuovo bridge: (a) from the Lastra a Signa, side and (b) details of the strengthening steel bars (beton plaquè technique) installed in the past.

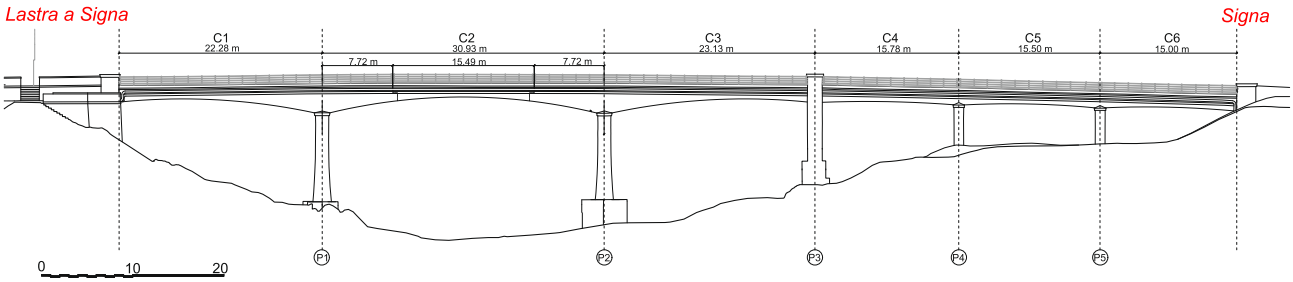

Fig. 2. (a) Drawing of the entire bridge and typical cross-sections: (b) at middle-span of C2 and (c) at the bearings P1 and P2.

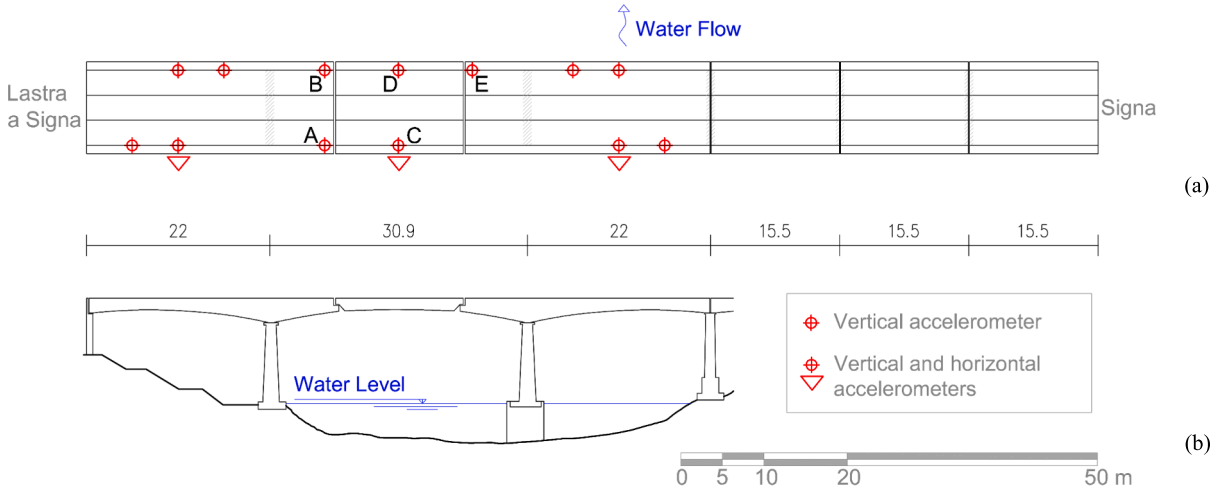

Fig. 3. (a) Plan of the sensor layout: the single red dot is a vertical monoaxial station, while the double dots are a biaxial station (measuring both vertical and horizontal); (b) Lateral view of the tested spans. (For interpretation of the references to colour in this figure legend, the reader is referred to the web version of this article.)

Table 1
The dynamic tests performed on the bridge and the testing environmental conditions.

Test	Length [s]	f_s [Hz]	Time [hh:mm]	T [°C]
T#1	700	1200	11:39	39.9
T#2	900	1200	11:58	39.7
T#3	880	2400	12:28	39.9

The position of the bridge is crucial because is the only crossing-point of the Arno River in the western suburbs of the Florentine area characterized by several industries and companies. As a consequence, the bridge is daily crossed by a high volume of vehicular traffic including heavy goods vehicles and line buses, each passing over the bridge at different speeds.

3.2. Dynamic test program

The experimental investigation was focused on the first three spans of the bridge. After a preliminary inspection, and with the aid of a finite element model, the sensor layout was defined as follows: sixteen PCB piezoelectric accelerometers (393-C, 393-B31 and 393-B12 models) were fixed on the opposite sidewalks to not interrupt the bridge service. Each span was equipped on three equally spaced sections (Fig. 3). Almost all the accelerometers were used to measure vertical accelerations; only three of them, placed at the middle of each span, were positioned to measure the accelerations in the transversal direction (i.e. the one orthogonal to the traffic direction).

Three sets of ambient vibration tests were performed on the 31st of July 2020. The first two measurements were recorded at a sampling frequency of 1200 Hz, while the last one at 2400 Hz. All the tests were performed around midday, in a relatively short time-span (about one hour); therefore, the environmental conditions can be reasonably considered constant for the three sets (Table 1). The duration of each set was about fifteen minutes, about 700 s, 900 s and 880 s for the tests

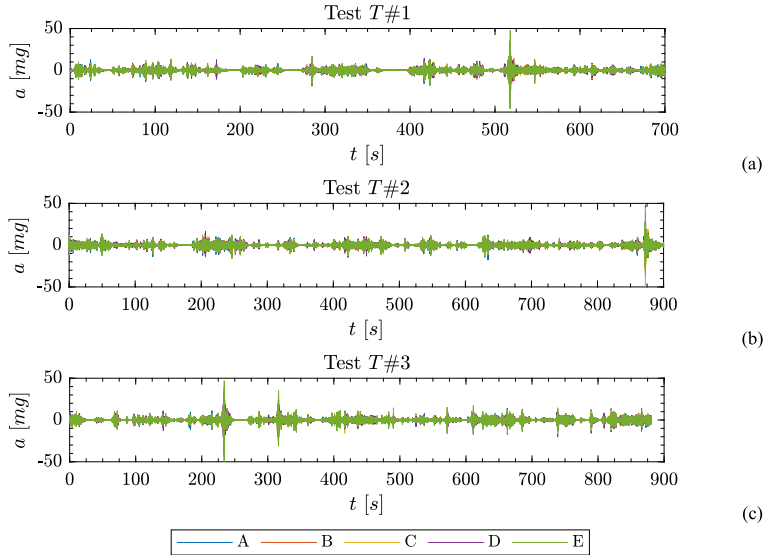

Fig. 4. Signals recorded and processed during the tests T#1 (a), T#2 (b) and T#3 (c).

hereafter referred as T#1, T#2 and T#3, respectively.

3.3. Signal processing

The experimental program was focused on the identification of the bridge modal parameters; thus, the accelerations were recorded simultaneously with the layout reported in Fig. 3. All the analyses were performed on signals with zero mean, filtered to remove noises at relatively very low or high frequencies. All the signals were firstly filtered by means of a third order Butterworth digital filter in the frequency band between 0.5 and 50 Hz (see f.i. Fig. 4). After checking for possible clipping and/or outliers, the signals were decimated until a Nyquist frequency of about 60 Hz.

Most of the dynamic identification were performed through the SSI-cov technique to attain a global damping value identified on the whole bridge (namely, global analysis). Aiming at investigating the role of the half-joint, the results were compared to those obtained with the RD technique on specific signals on the second span of the bridge (namely, local analysis).

3.4. Dynamic identification

The modal parameters of the bridge were estimated on the three sets collected during the experimental program considering the full length of the signals (with respect to time). The SSI-cov was used as the reference technique to estimate frequency, damping and mode shape, while FDD and RD techniques were used to check the results. In Fig. 5 the results of both FDD and SSI are reported in the frequency band between 0.5 and 50 Hz.

The values obtained for the three sets were very similar, therefore in Table 2 only the first 10 modes identified in T#3 are reported.

In this table, for the first two modes, a weighted average value of the damping estimated by means of the RD technique is also reported. Considering thirteen time-histories (therefore, disregarding the results of the three horizontal accelerometers measuring in the transversal direction) the first two damping ratios calculated with the RD technique exhibit values between 0.0195 and 0.0211. Therefore, with the aim to give more weight to the results obtained where the signal amplitude was greater (for a specific mode), and hence the signal-to-noise ratio was supposedly better, a weight function based on the mode shapes (as estimated from the FDD analysis) was used. Thus, considering n measured DOFs, the k-th mode averaged damping ratio $\widehat{\xi}_k$ is calculated as reported in the following Eq. (7):

$$\widehat{\xi}_k = \frac{\sum_{j=1}^{n} \xi_j^{(k)} \phi_j^{(k)}}{\sum_{i=1}^{n} \phi_i^{(k)}}. \tag{7}$$

According to the criterion reported in Section 2, the RD was applied to the filtered signals around the peaks corresponding to the first and second modes, considering a frequency band of (f_1-1.04, f_1+0.44) Hz

Table 2
The first 10 modes (T#3 test) identified with different techniques.

Mode	*SSI-cov*		*FDD*	*RD*
	$\mu(f_n)$ [Hz]	$\mu(\xi_n)$ [%]	f_n [Hz]	ξ_n [%]
#01	3.16	2.30	3.19	2.00
#02	4.61	2.20	4.61	1.92
#03	7.38	1.31	7.32	–
#04	7.68	2.59	–	–
#05	8.33	2.40	8.24	–
#06	8.93	1.98	8.97	–
#07	10.23	2.32	10.40	–
#08	12.45	2.28	12.45	–
#09	12.74	1.67	–	–
#10	13.39	2.07	13.7	–

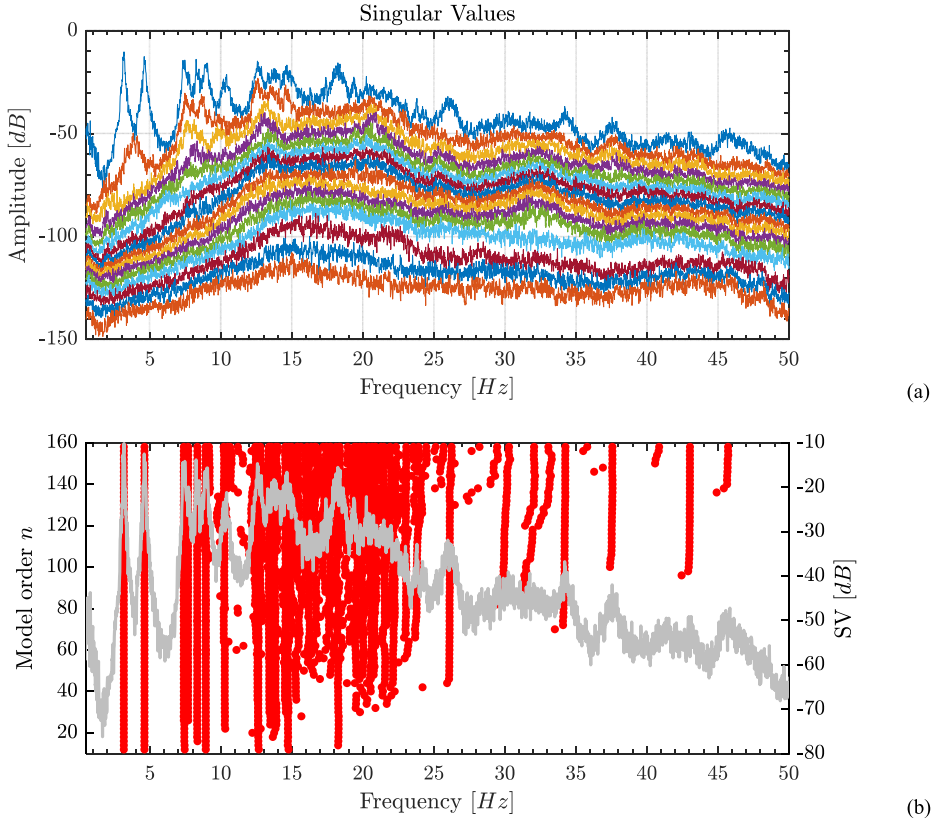

Fig. 5. Results of the dynamic identification of T#3: (a) The singular values of the PSD matrix and (b) the stabilization chart.

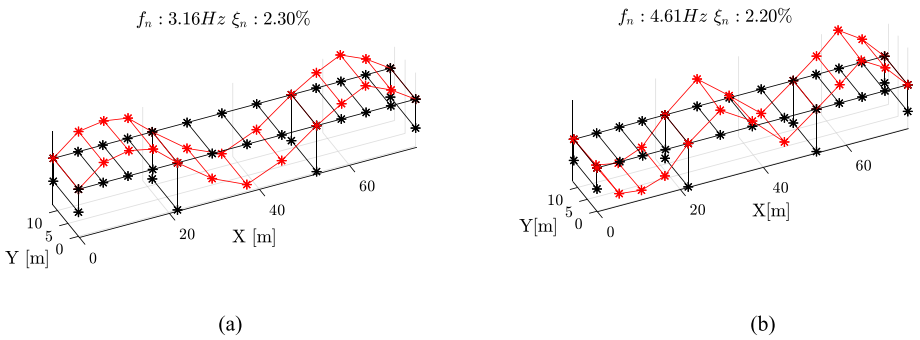

Fig. 6. (a) Fist and (b) second mode identified through the SSI-cov.

and (f_2-0.46, f_2+0.95) Hz, respectively. The method was used by fixing a positive level crossing equal to $\sqrt{2}\sigma_x$ (where σ_x is the standard deviation of the analysed signal), and a segment time length equal to 3 s.

By contrast, the FDD technique [32] was used to check the signal-to-noise ratio during the tests and to verify the identified modal parameters with the SSI-cov technique during the post-processing phase. Despite the well-known limits of this technique for closely spaced modes (e.g. [24]), the Singular Value Decomposition (SVD) of the Power Spectral Density (PSD) matrix can be considered a reliable method to have a quick insight on the results obtained with the SSI-cov. Moreover, the FDD is a frequency-based method which does not require any parameter setting phase, but only a visual inspection of the PSD matrix components. The PSD matrix was estimated by means of the Welch's function implemented in Matlab®, performing the Fourier transform on 2^{16} points (the number was fixed after a stationarity convergence check) over signal windows with an equal number of samples, and overlapping the window selection by 66% after a Hanning windowing to avoid leakage effects.

In the following, this study will mainly consider the first two modes involving the central span C2. For the sake of clarity, in Fig. 6 are reported the mode shapes identified with the SSI technique fed with the signal covariance.

4. Results

4.1. Effects of the signal length

The length of the signal [33] plays a key role in the accuracy of the damping estimation during ambient vibration tests. On the one hand the signal length should be long enough to guarantee a suitable number of cycles in the first mode correlation function; on the other hand, the hypothesis of Gaussian white-noise input [34] should be satisfied to limit the bias on the results. Considering the first two modes, the effect of the signal length on the estimation of the modal parameters is investigated by using an increasing time window. The starting point of each window is fixed at the time step $t_0 = 0$, while the ending point $t_f = t_0 + k\Delta t$ is shifted with $\Delta t = 10\ s$ corresponding to larger sample size at each *k-step*. Thus, the SSI-cov technique is used to identify the modal parameters over the defined time window $t_w = [t_0, t_f]$. The results of such sensitivity analysis are reported in Fig. 7 in terms of frequencies, and in Fig. 8 in terms of damping ratios for the investigated modes.

From the very first points, the variation interval for the first two identified frequencies is almost negligible (about 0.188 Hz and 0.224 Hz, respectively). On the contrary, the damping ratio exhibits different behaviours, depending on which mode is observed. While for the second mode a convergence to stable values is reached for all the tests (T#1, T#2 and T#3), the damping ratio of the first mode exhibits different patterns: (i) in T#1 it raises and plunges, stabilizing only for limited time spans, (ii) in T#2 it exhibits a negative trend as the sample size increases, stabilizing to a constant value only after 470 s. A further different behaviour can be observed (iii) in T#3, whereby the damping does not reach a constant value after t_f equal to 300 s but exhibits a slight negative slope until the end of the signal.

During the tests, the minimum length of the signals is defined a-priori to assure a good representation of the lowest resonant-frequency. Commonly, the following rule of thumb providing the minimum value as a function of the first mode modal properties (ξ_1, f_1) is adopted [24]:

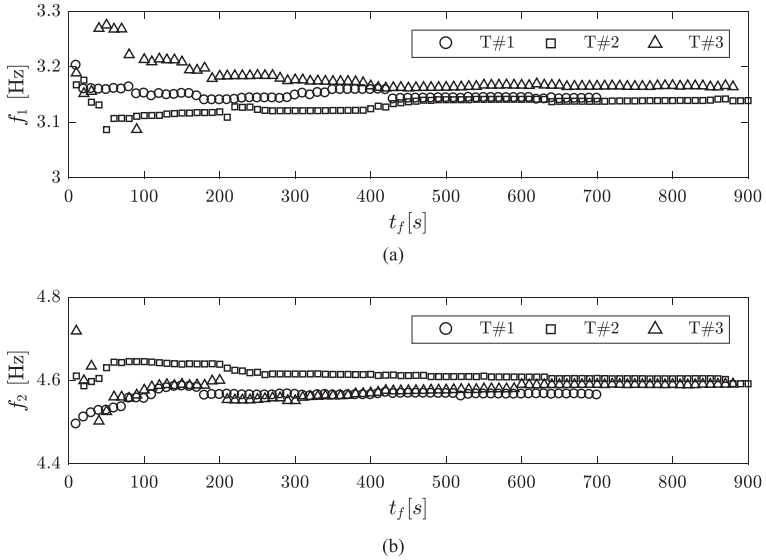

Fig. 7. The identified frequencies for different signal lengths t_w in T#1, T#2 and T#3 tests. The first two modes are analysed: (a) First mode and (b) Second mode.

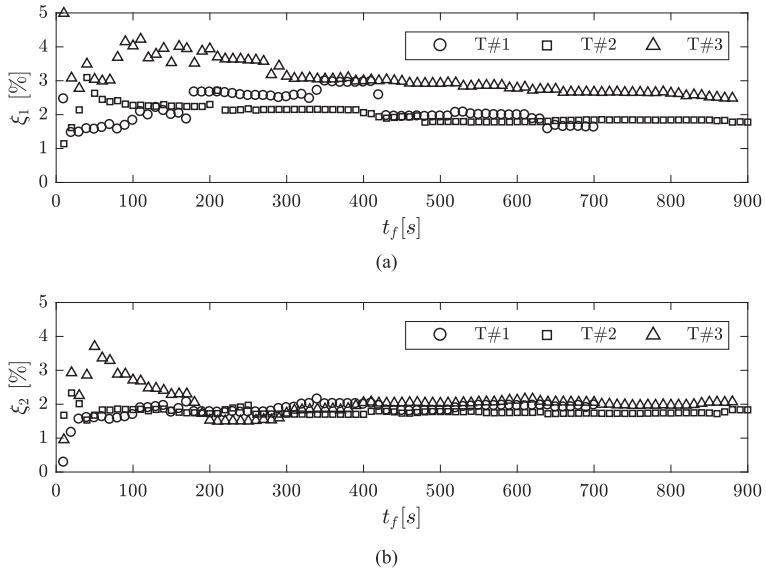

Fig. 8. The identified damping ratios for different signal lengths t_w in T#1, T#2 and T#3 tests. The first two modes are analysed: (a) First mode and (b) Second mode.

$$T_{tot} > \frac{10}{\xi_1 f_1}. \tag{8}$$

By using Eq. (8), the total time-series length T_{tot} allows to estimate about 20 times the time lag of the correlation function of the lowest frequency of interest. According to this rule, and assuming a damping ratio equal to 1% and a frequency of 3 Hz, a measure of about 350 s can be considered long enough to obtain reliable results in operational modal analysis.

Interestingly, only in the second mode (see Fig. 8) the convergence is reached at $t_w = 350$ s in all the three tests (T#1, T#2 and T#3). On the contrary, the first mode exhibits relatively chaotic patterns, and only in one case (T#2) the convergence is reached at the reference time of about T_{tot}.

To have an insight on the local behaviour of the bridge during T#1, the signals of some selected accelerometers were analysed and individually processed by means of the RD technique. In particular, the analysis was focused on the accelerometers mounted across the half-joints (labelled from A to E in Fig. 3). For the first mode all the sensors from A to E were analysed, while only A, B, E were considered for the second mode (given the mode shape, the sensors in locations C and D are nodes, and they were not considered in the analysis).

As shown in Fig. 9, besides the difference expected by using a different damping estimation technique, the local analysis confirms the previously observed behaviour: after 300 s, the damping jumps up to values around 3%, suddenly reduced to 2.5%, to then finally decrease rapidly down to 2%. On the contrary, the second mode after 300 s has almost constant damping of about 2%. Interestingly, in this case, the damping ratios are bounded by the results obtained in stations B and E (at the half-joints on the downstream side of the bridge). This behaviour was not observed in the first mode: only from 420 s onwards the boundary values are represented by the damping ratios identified in the station E and A (at the sections before the half-joints), respectively.

4.2. Time-damping analysis

Aiming to investigate more in depth the sensitivity of the estimated modal parameters with respect to the length of the selected window, an additional analysis was performed by means of a moving window over the signals. In particular, three different window lengths (L) of 100, 200 and 300 s were chosen. Each window moves forward in the signal, with 50% overlapping to estimate the damping ratio along the different parts of the signals. Considering that the vehicular traffic composition is not constant over time, this time-damping analysis can also provide more information about the effects of the load variability on the damping estimation. It is worth observing that the length of the moving time windows was selected to have values around T_{tot}. that can be obtained from a preliminary estimation (about 330 s) and with the identified values (about 140 s).

In Fig. 10, the results for each test are represented by means of markers to distinguish the different window lengths, while the cumulative results of damping estimation calculated with the window t_w (as those reported in Fig. 7) are shown in grey.

The results of the first damping ratio in T#1 seem to confirm the pattern previously observed in Fig. 8 and Fig. 9. The second mode shows a similar behaviour, even if the identified damping values range in a smaller interval, exhibiting a lower dependence on the selected time-window lengths. Moreover, some peculiarities can be reported for t_w

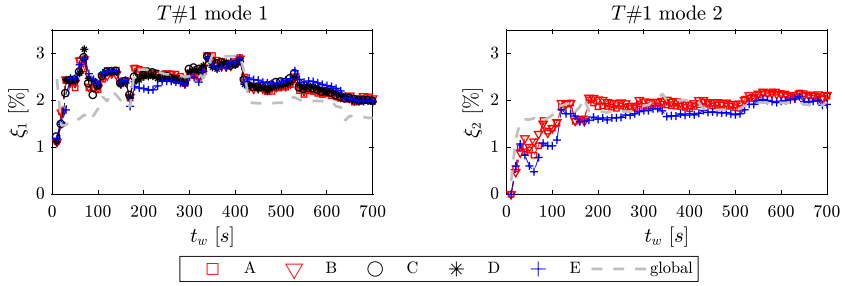

Fig. 9. Damping identified at some selected accelerometers (the grey line represents the global results) for the first two modes during the T#1 test.

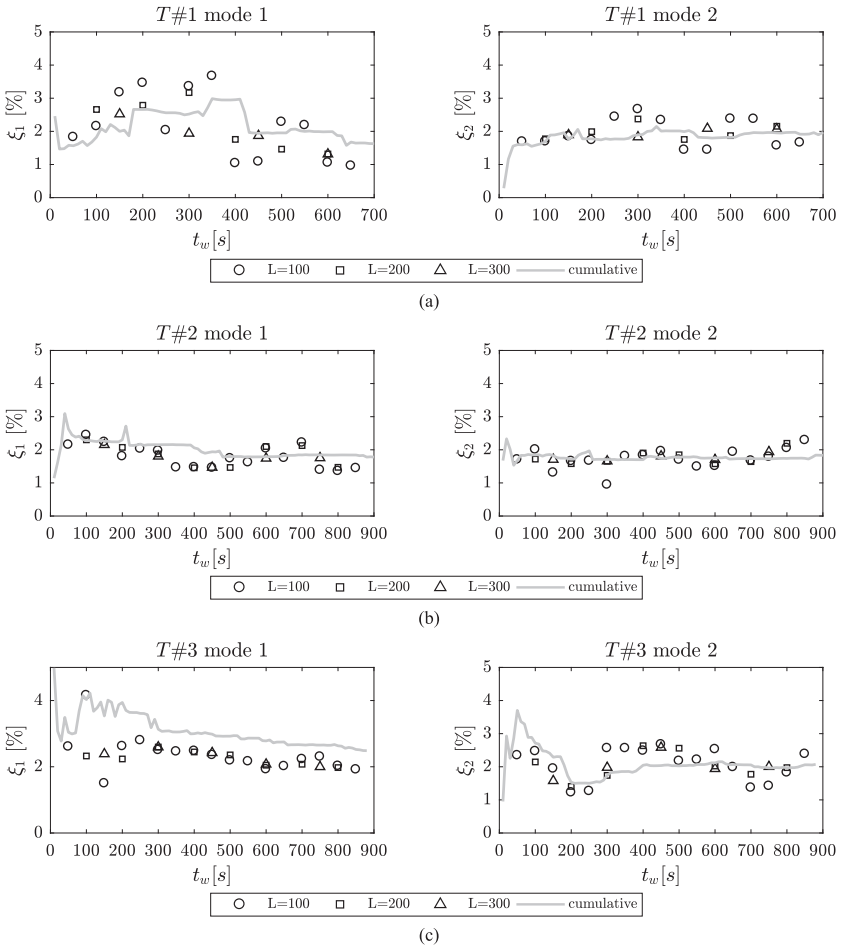

Fig. 10. The identified damping ratios with moving windows of different lengths respectively for the tests: (a) T#1 (b) T#2, and (c) T#3. In grey the cumulative results attained with the raising t_f values showed in Fig. 8.

Table 3
The range of the values identified in each test for each moving-window length.

Test	**Window length [s]**	*Mode 1*		*Mode 2*	
		$min(\xi_n)$ **[%]**	$max(\xi_n)$ **[%]**	$min(\xi_n)$ **[%]**	$max(\xi_n)$ **[%]**
T#1	*100*	0.96	3.67	1.44	2.67
	200	1.46	3.17	1.76	2.37
	300	1.31	2.52	1.83	2.08
T#2	*100*	1.36	2.45	0.94	2.09
	200	1.45	2.30	1.58	2.20
	300	1.46	2.15	1.71	1.94
T#3	*100*	1.50	4.16	1.22	2.67
	200	2.23	2.45	1.41	2.64
	300	2.00	2.59	1.58	2.58

equal to 300 and 600 s (i.e. where it is possible to compare the results obtained with the three different moving windows). For $t_w = 300$ s, the damping values obtained with the windows of 100 and 200 s are almost equal, while considering a moving window of 300 s the estimated value is much lower. Conversely, for $t_w = 600$ s, the values attained from the three windows are almost the same.

The T#2 test, reported in Fig. 10-b, exhibits an analogous behaviour for the two investigated modes except for the values identified at t = 300 s in the second mode, with the moving window of 100 s. The damping estimated on the moving windows acceptably complies with the results obtained with the increasing window.

Figure 10-c shows that for the T#3 test, for both the investigated modes, the damping values are close regardless of the used time-window length. Only in the first mode, using the smallest time window, two discontinuities are visible respectively at t_w equal to 100 and 150 s. Moreover, it is worth noting that also on the second mode, at $t_w = 300$ s, the damping obtained with the 100 s moving window is different from the other two cases (L = 200 and 300 s).The values obtained for the first mode in T#3 test with the moving windows, if compared to the damping estimated with the increasing window (grey line), are always lower

(Fig. 10-c).

Table 3 quantifies the interval of the estimated damping ratio for each moving window. While locally the main differences among the different time-window lengths can be mainly found in the first mode during T#1 test (see Fig. 10-a), a considerable variation over time can be observed in all the tests. In particular, the variation interval of the estimated damping reaches 3% and 1.5% in the first and second modes, respectively.

5. Discussion of the results

5.1. Influence of the window length

Considering the behaviour observed in damping estimation by varying the sample size, the differences between consecutive values (and with respect to a reference value, specifically the one corresponding to T_{tot}) were considered for a better understanding of this phenomenon.

Fig. 11 shows the damping ratio for the increasing time window (the same reported in Fig. 8) with respect to the difference between two consecutive values. In particular, the relative error Δ_k (expressed as percentage) at the k-th step, is calculated as follows:

$$\Delta_k = \frac{|\xi_k - \xi_{k-1}|}{\xi_{k-1}}. \tag{9}$$

Obviously, if the damping values stabilize to a constant value, Δ_k will approach zero, confirming a convergence to a minimum sample size. A practical solution to identify an acceptable window length $\widetilde{L}_w$ can be found by fixing a threshold of acceptance (for instance $\widetilde{\Delta} = 10\%$) and finding the k-th time t_k where the convergence criterion $\Delta_k < \widetilde{\Delta}$ is satisfied for the entire signal length.

Considering the second mode, a convergence can be easily obtained for every set (T#1, T#2 and T#3) with values ranging from 170 s to 250 s (see Table 1). Conversely, for the first mode a convergence cannot be found in T#1, while in the other two tests (T#2 and T#3) values of 470 s and 270 s can be found, respectively. On the one hand, these results show that higher window lengths are required for the first mode because of the longer correlation time in the response of the lowest frequency. On the other hand, the behaviour observed in the first mode during the T#1 test implies that some phenomena activating higher damping ratios are possibly occurring between 330 s and 430 s (or some errors may arise due to the non-stationarity of the process).

It is worth to notice that, even if during T#3 test a convergence is achieved after 270 s, with very small distances, those values are always of the same sign. Thus, the cumulative distance is always consistent, and the convergence criterion cannot be satisfied.

All the results of the optimal length $\widetilde{L}_w$ defined with the criterion described above, are reported in Table 4 for the first two modes of each test.

Lastly, a comparison between the damping ratios computed in all the time windows and the reference value according to the literature is re-

Table 4
Window length $\widetilde{L}_w$ [s] of last threshold crossing for each measurement set.

Mode	T#1	T#2	T#3
#01	–	470	270
#02	170	250	190

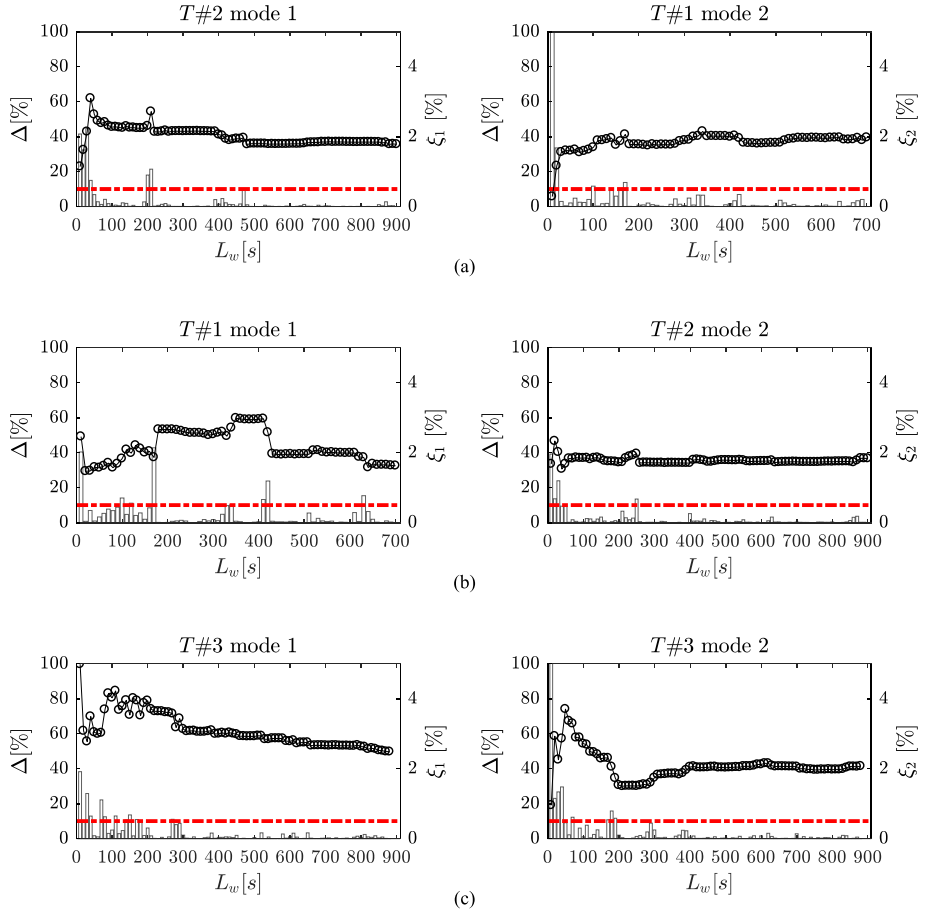

Fig. 11. Plots of the relative errors Δ (the red line represents a relative error threshold$\widetilde{\Delta} = 10\%$): (a) T#1, (b) T#2 and (c) T#3. (For interpretation of the references to colour in this figure legend, the reader is referred to the web version of this article.)

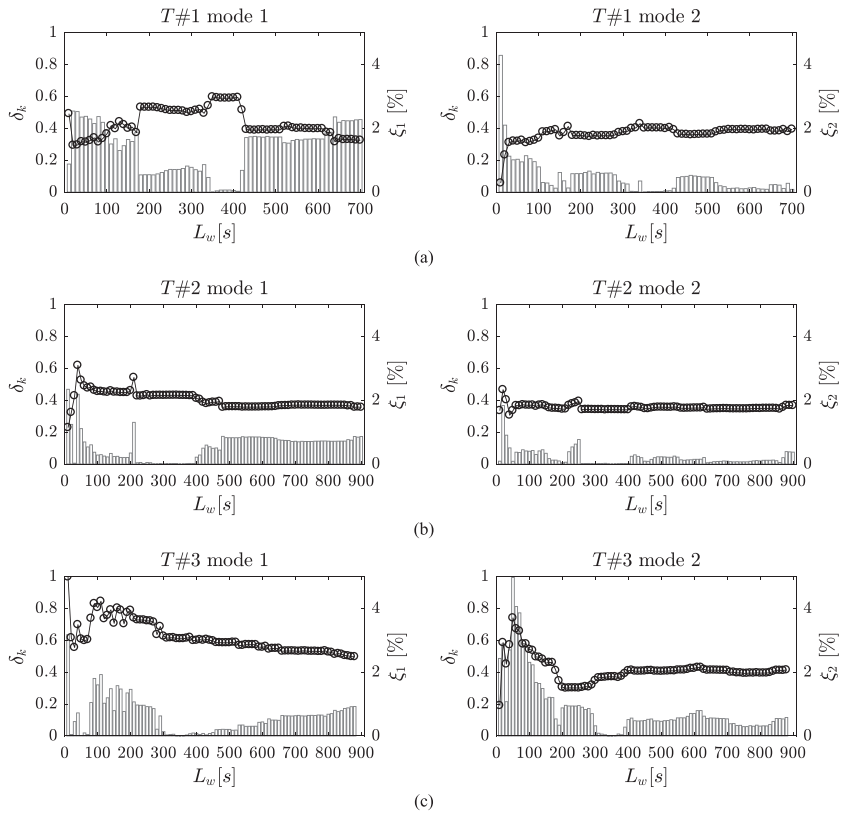

Fig. 12. The relative errors δ_k between the damping ξ_{ref} estimated in the reference window length $\underline{L_w}$ and the damping ξ estimated in a window length L_w during; (a) T#1, (b) T#2 and (c) T#3.

ported. As introduced in Section 3.1, a reference time window $\underline{L_w}$ equal to 350 s can be considered. Therefore, in Fig. 12, the damping ratio (ξ_{ref}) estimated on a signal length equal to $\underline{L_w}$ is compared with ξ_k estimated in the k-th window length L_k, to analyse the relative distance δ_k.

$$\delta_k = \frac{|\xi_k - \xi_{ref}|}{\xi_{ref}}. \tag{10}$$

While below $\underline{L_w}$ larger distances are expected due to shorter correlation time, a huge reduction of these differences may be observed for longer time-windows. Whereas such behaviour is not exhibited, especially in the first mode with relative distances ranging from 0.07 to 0.45, a sort of convergence can be observed for the second mode with values of δ_k lower than 0.15. For instance, in Fig. 12 the first mode exhibits values of δ_k up to 0.45 both for windows smaller and larger than $\underline{L_w}$. A similar behaviour can be observed in T#2 (Fig. 12-b) and T#3 (Fig. 12-c), although the relative distances are halved with respect to T#1.

5.2. Damping correlation with the vibration signatures

The damping variations obtained with respect to the signal time length were compared to other parameters characterizing the signals. In particular, the results of the moving windows tests were correlated with some statistical properties of the recorded accelerations such as root mean square, maximum value, and kurtosis.

The analyses were distinguished based on the time-length of the moving window, i.e. for each moving window (L = 100, 200 and 300 s) the results from all the three tests (T#1, T#2 and T#3) are used. A first attempt performed on the raw signals was not able to show a possible relation between the obtained damping and the signal properties. Then, the correlations were repeated with the statistical moments computed on filtered signals, by using the frequency bands previously selected in the RD analyses, namely (f_1-1.04, f_1+0.44) Hz and (f_2-0.46, f_2+0.95) for the first and the second mode. As reported in Fig. 13, a weak correlation was found between damping and both rms and peak accerelation of the filtered signal. The results obtained for a time window equal to 200 s (Fig. 13) are quite similar to those obtained with the 300 s time windows, although the latter exhibit a slightly stronger correlation for the first mode and a smaller coefficient of determination for the second one. Conversely, with a time length equal to 100 s, the correlations are lower than those for 200 or 300 s in both the analysed modes.

Although the correlation between the damping and the rms was not very strong, the comparison between these quantities, evaluated according to an increasing signal length seems to provide a way to understand the damping variations over the signals. Hence, an additional way to represent their relation is presented by means of the following parameters:

$$\Delta_\xi = \frac{\xi_k - \xi_{ref}}{\xi_{ref}}, \tag{11}$$

$$\Delta_{rms} = \frac{rms_k - rms_{ref}}{rms_{ref}}. \tag{12}$$

As shown in Fig. 14, starting from the reference time length of 350 s, the peculiar behaviour observed in T#1 test follows the variation of rms (Δ_{rms}). In T#2 test, Δ_{rms} fluctuates around 0.1, and after $t_w = 500$ s the corresponding difference in damping is almost constant. Lastly, test T#3 exhibits a Δ_{rms} lower than 0.1, and the correlation between damping and rms appears weak. Thus, the correlation between damping and rms of the filtered signal is increasing above a certain threshold value.

The identified damping values with feeble signals are more sensitive to the lower mass values of the dynamic system (bridge without vehicular traffic) than to the vibration amplitude, while above a certain rms value the additional mass (constant vehicular traffic) on the bridge is

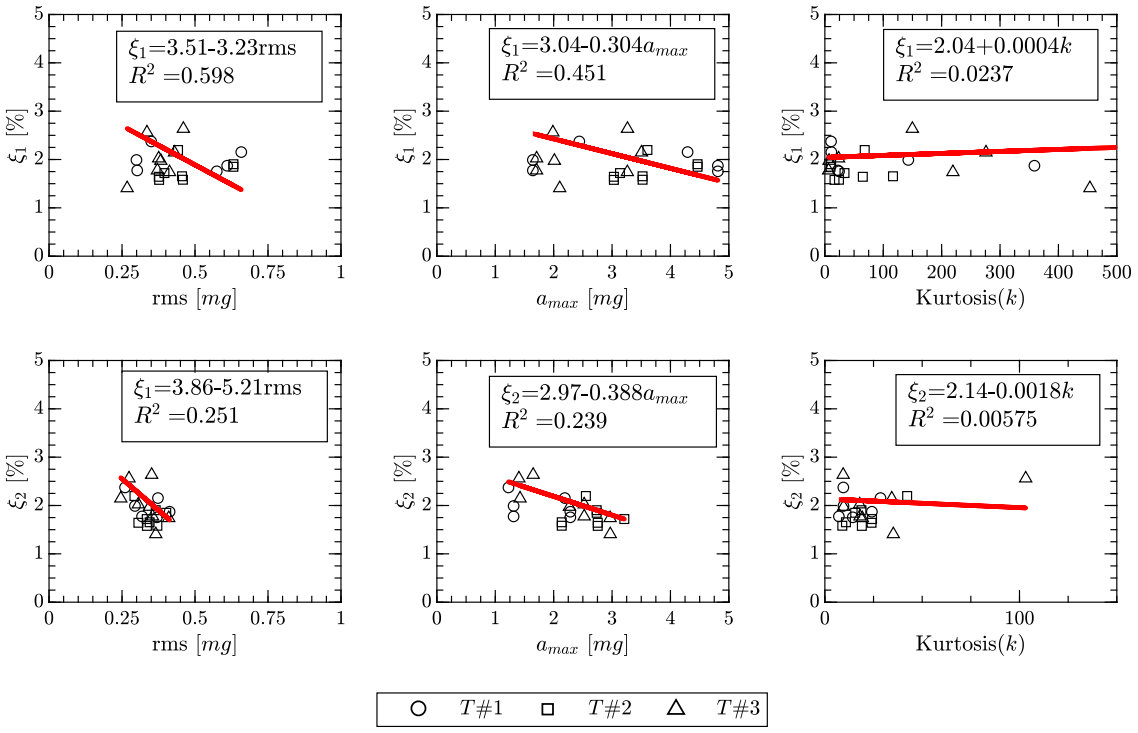

Fig. 13. Correlation of the damping evaluated on time windows of 200 s and the vibration signatures filtered around the first and the second mode frequencies.

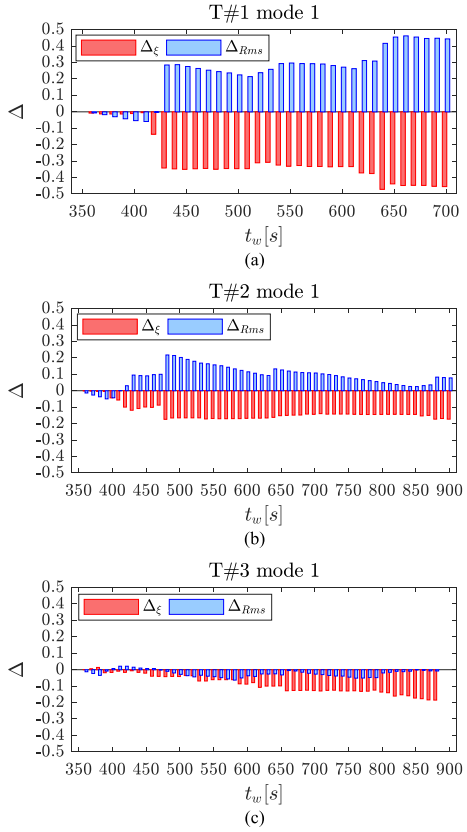

Fig. 14. Comparison between Δ_{rms} and Δ_k in the first mode for the tests: (a) T#1, (b) T#2 and (c) T#3.

almost constant and the damping value is mainly influenced by the vibration amplitude, activating some extra energy dissipation mechanisms.

6. Conclusive remarks

Even if the damping ratio is a key parameter to assess the structural integrity of bridges and their response under traffic vibrations, to date only few studies investigated the damping estimation on bridges, and none of them consider the short-span RC bridges with half-joint beams. Aiming to contribute to fill this gap, this paper analyses and discusses the results of an experimental program performed on a RC bridge in Italy (near Florence). This investigation was focused on the estimation of the damping of the first two modes and, different identification parametric and non-parametric technique were employed (RD, SSI-cov).

The analysis of the results highlights how the damping ratio estimation might be affected by some bias, due to the nature of the traffic-induced vibrations and to the minimum sample size required to represent the lowest resonant frequency. This means that the definition of a proper time length for the dynamic measurements on in-service bridges cannot be easily quantified through the existing heuristic rules of thumb. On the other hand, the results showed the existence of a negative correlation - albeit weak - between the power of signals (rms and peak acceleration of the filtered signal) and the damping ratio. Although the correlation found is not very strong, the comparison between these quantities evaluated according to an increasing signal length provides a way to understand the damping variations over the signals.

Future studies on larger dataset of short-span RC bridges are needed to confirm the results reported and discussed here. Moving toward this direction, additional effort is required to include the higher modes to improve characterization of bridges' local behaviours under traffic loads that can provide a further inside on the damping ratios behaviour.

CRediT authorship contribution statement

Giacomo Zini: Conceptualization, Investigation, Methodology, Writing – review & editing. **Andrea Giachetti:** Conceptualization,

Investigation, Methodology, Writing – review & editing. **Michele Betti:** Conceptualization, Investigation, Methodology, Writing – review & editing. **Gianni Bartoli:** Conceptualization, Investigation, Methodology, Writing – review & editing.

Declaration of Competing Interest

The authors declare that they have no known competing financial interests or personal relationships that could have appeared to influence the work reported in this paper.

Data availability

Data will be made available on request.

Acknowledgements

The authors acknowledge the municipality of Signa and Lastra a Signa for the availability in carrying out the experimental tests.

References

[1] Calvi GM, Moratti M, O'Reilly GJ, Scattarreggia N, Monteiro R, Malomo D, et al. Once upon a Time in Italy: The Tale of the Morandi Bridge. Struct Eng Int 2019;29:198–217. https://doi.org/10.1080/10168664.2018.1558033.
[2] Marcheggianni L, Clementi F, A.. Formisano Static and dynamic testing of highway bridges: a best practice example, Journal of Civil. Struct Health Monit 2020;10:43–56. https://doi.org/10.1007/s13349-019-00368-1.
[3] Marcheggiani L, Clementi F, Formisano A, Dynamic Identification and Monitoring of a New Highway Bridge, in: 2021: pp. 603–617. doi:10.1007/978-3-030-74258-4_39.
[4] Yamaguchi H, Matsumoto Y, Kawarai K, Dammika AJ, Shahzad S, Takanami R, Damage detection based on modal damping change in bridges, ICSBE-2012: International Conference on Sustainable Built Environment, Kandy, Sri Lanka, 14-16 December 2012 (2012).
[5] Grillanda N, Milani G, Ghosh S, Halani B, Varma M. SHM of a severely cracked masonry arch bridge in India: Experimental campaign and adaptive NURBS limit analysis numerical investigation. Constr Build Mater 2021;280:122490. https://doi.org/10.1016/j.conbuildmat.2021.122490.
[6] Zarafshan A, Ansari F, Taylor T. Field tests and verification of damping calculation methods for operating highway bridges, Journal of Civil. Struct Health Monit 2014;4:99–105. https://doi.org/10.1007/s13349-013-0067-y.
[7] Cunha A, Caetano E, Delgado R. Dynamic tests on large cable-stayed bridge. J Bridg Eng 2001;6:54–62. https://doi.org/10.1061/(ASCE)1084-0702(2001)6:1(54).
[8] Conte JP, He X, Moaveni B, Masri SF, Caffrey JP, Wahbeh M, et al. Dynamic Testing of Alfred Zampa Memorial Bridge. J Struct Eng 2008;134:1006–15. https://doi.org/10.1061/(asce)0733-9445(2008)134:6(1006).
[9] Brownjohn JMW, Magalhaes F, Caetano E, Cunha A. Ambient vibration re-testing and operational modal analysis of the Humber Bridge. Eng Struct 2010;32:2003–18. https://doi.org/10.1016/j.engstruct.2010.02.034.
[10] Jones NP, Spartz CA. Structural damping estimation for long-span bridges. J Eng Mech 1990;116:2414–33. https://doi.org/10.1061/(ASCE)0733-9399(1990)116:11(2414).
[11] Nagayama T, Abe M, Fujino Y, Ikeda K. Structural Identification of a Nonproportionally Damped System and Its Application to a Full-Scale Suspension Bridge. J Struct Eng 2005;131:1536–45. https://doi.org/10.1061/(asce)0733-9445(2005)131:10(1536).
[12] Lee S, Feng MQ, Kwon S-J, Hong S-H. Equivalent Modal Damping of Short-Span Bridges Subjected to Strong Motion. J Bridg Eng 2011;16:316–23. https://doi.org/10.1061/(asce)be.1943-5592.0000149.
[13] Schubert S, Gsell D, Steiger R, Feltrin G. Influence of asphalt pavement on damping ratio and resonance frequencies of timber bridges. Eng Struct 2010;32:3122–9. https://doi.org/10.1016/j.engstruct.2010.05.031.
[14] Morassi A, Tonon S. Dynamic Testing for Structural Identification of a Bridge. J Bridg Eng 2008;13:573–85. https://doi.org/10.1061/(asce)1084-0702(2008)13:6(573).
[15] Bayraktar A, Altunişik AC, Türker T. Structural condition assessment of Birecik highway bridge using operational modal analysis. Int J Civil Eng 2016;14:35–46. https://doi.org/10.1007/s40999-016-0010-9.
[16] Gentile C. Modal and structural identification of a R.C. arch bridge. Struct Eng Mech 2006;22:53–70. https://doi.org/10.12989/sem.2006.22.1.053.
[17] Lorenzoni F, De Conto N, da Porto F, Modena C. Ambient and free-vibration tests to improve the quantification and estimation of modal parameters in existing bridges. J Civ Struct Heal Monit 2019;9:617–37. https://doi.org/10.1007/s13349-019-00357-4.
[18] Li P-F, Wang Y-F, Liu B-D, Su L. Damping Properties of Highway Bridges in China. J Bridg Eng 2014;19:04014005. https://doi.org/10.1061/(asce)be.1943-5592.0000578.
[19] Gutenbrunner G, Savov K, Wenzel H. Sensitivity Studies on Damping Estimation, Proceedings of the Second International Conference of Experimental Vibration Analysis for Civil Engineering Structures, EVACES, Porto, 24-26 October 2007 (2007). http://www.vce.at/pdf/downloads/Publications/Damping Estimation.pdf.
[20] Cole H.A. On-line failure detection and damping measurement of aerospace structures by random decrement signatures, No. NASA-CR-2205. NASA, (1973).
[21] Van Overschee P, De Moor B. Subspace Identification for Linear Systems, Holanda: Kluwer Academic Publishers, Dordrecht, (1996) doi:10.1007/978-1-4613-0465-4.
[22] Farrar CR, James GH. System identification from ambient vibration measurements on a bridge. J Sound Vib 1997;205:1–18. https://doi.org/10.1006/jsvi.1997.0977.
[23] Caughey TK, O'Kelly MEJ. General theory of vibration of damped linear dynamic systems. California Institute of Technology; 1963.
[24] Brincker R, Ventura CE. Introduction to Operational Modal Analysis. John Wiley & Sons 2015. https://doi.org/10.1002/9781118535141.
[25] Brandt A. Noise and Vibration Analysis: Signal Analysis and Experimental Procedures. John Wiley & Sons 2011. https://doi.org/10.1002/9780470978160.
[26] Jeary AP. Damping in tall buildings—a mechanism and a predictor. Earthq Eng Struct Dyn 1986;14:733–50. https://doi.org/10.1002/eqe.4290140505.
[27] Rodrigues J, Brincker R. Application of the random decrement technique in operational modal analysis, Proceedings of the First International Operational Modal Analysis Conference, Copenhagen IOMAC 2005. (2005).
[28] Allemang RJ. The modal assurance criterion - Twenty years of use and abuse. Sound Vib 2003;37:14–21.
[29] Magalhães F, Cunha Á. Explaining operational modal analysis with data from an arch bridge. Mech Syst Sign Process 2011;25:1431–50. https://doi.org/10.1016/j.ymssp.2010.08.001.
[30] Zini G, Betti M, Bartoli G. A quality-based automated procedure for operational modal analysis. Mech Syst Sign Process 2022;164:108173. https://doi.org/10.1016/j.ymssp.2021.108173.
[31] Mugnai F, Bonora V, Tucci G. Integration, harmonization, and processing of geomatic data for bridge health assessment: the Lastra a Signa case study. Appl Geom 2023. https://doi.org/10.1007/s12518-023-00510-1.
[32] Brincker R, Zhang L, Andersen P. Modal identification of output-only systems using frequency domain decomposition. Smart Mater Struct 2001;10:441–5. https://doi.org/10.1088/0964-1726/10/3/303.
[33] Pridham BA, Wilson JC. A study of damping errors in correlation-driven stochastic realizations using short data sets. Probab Eng Mech 2003;18:61–77. https://doi.org/10.1016/S0266-8920(02)00042-5.
[34] Daems PJ, Peeters C, Guillaume P, Helsen J. Removal of non-stationary harmonics for operational modal analysis in time and frequency domain. Mech Syst Sign Process 2022;165:108329. https://doi.org/10.1016/j.ymssp.2021.108329.